Coherent dynamics of bipolaritons in bulk CdS

Ch. Mann, W. Langbein, and U. Woggon
FB Physik, Universität Dortmund, Otto-Hahn Str. 4, D-44221 Dortmund, Germany

A. L. Ivanov
Department of Physics and Astronomy, Cardiff University, Wales, United Kingdom
(Received 25 June 2001; published 27 November 2001)

The coherent dynamics of an optically driven exciton–photon–bipolariton system is studied in bulk CdS. Applying backward-scattering four-wave mixing (FWM) spectroscopy, we analyze the two-photon polarization associated with excitonic molecules and determine the dephasing time $T_2 \simeq 4.8$ ps. We demonstrate that the molecule-mediated FWM signal persists at positive time delays even in the $\chi^{(3)}$ limit, due to the spatial pinning of coherent polaritons induced by the second pulse. By generalizing the bipolariton model to uniaxial semiconductors, we calculate $\tau_{\mathrm{rad}}^{XX} \simeq 2.8$ ps, justify the $T_2 = 2T_1$ limit, and prove the bipolariton representation for excitonic molecules in CdS.

DOI: 10.1103/PhysRevB.64.235206 PACS number(s): 71.35.−y, 71.36.+c, 78.55.−m, 33.80.−b

I. INTRODUCTION

Resonantly interacting excitons and photons give rise to polariton eigenstates in solids.[1] Consequently, the optical properties of excitonic molecules (XXs) can be described in terms of polariton–polariton interaction, i.e., by the scheme ''two polaritons $\leftrightarrow XX$'' which results in the bipolariton representation of XXs.[2] Since the observation of photoluminescence of excitonic molecules in CuCl,[3] this semiconductor became a prototype material in optics of molecules, due to its optical isotropy and the large XX binding energy. The optics of excitonic molecules in hexagonal semiconductors, like CdS or CdSe, is more sophisticated and much less developed because of the anisotropy in the exciton–photon transition.[4] At present, the polariton concept is extended to semiconductor microcavities and very recent studies address even the problem of cavity bipolaritons for semiconductor nanostructures.[5–8] Although the bipolariton eigenstate is a basic elementary excitation in solids, the optical properties of these quasiparticles are not fully understood yet, mainly due to the lack of relevant experimental data. Except from bulk CuCl,[4,9–12] the bipolariton picture of excitonic molecules has not been experimentally verified for other materials, and almost no information is available about the coherent dynamics in the coupled exciton–photon–bipolariton system.

For optically isotropic semiconductors, the bipolariton model interprets an excitonic molecule as two quasibound σ^+ and σ^--polarized polaritons provided that both exciton–exciton Coulombic interaction (attraction) and the exciton–photon coupling (polariton effect) are treated simultaneously and beyond low-order perturbation theory.[2] The bipolariton concept implies a hierarchy of interactions: The coupling of molecules with the light field should be stronger than any other scattering process. This means that the decay of the two-photon polarization associated with excitonic molecules is mainly determined by the radiative decay of XXs (the $T_2 = 2T_1$ limit). In particular, the optical decay of molecules should dominate over XX-phonon scattering. In spite of the long radiative lifetime of excitonic molecules in bulk CuCl, $\tau_{\mathrm{rad}}^{XX} \simeq 20$ ps, the bipolariton representation is valid for this semiconductor[2], due to an anomalously weak exciton–phonon interaction in CuCl.[13] As we will show below, the bipolariton picture is also valid for excitonic molecules in bulk CdS at low temperatures, because the radiative lifetime of the molecules is about 3 ps, while the relevant scattering time due to exciton–LA–phonon interaction refers to a 10 picosecond time scale.[14–16]

Within the bipolariton picture the sequence ''two incoming (σ^+ and σ^-) photons→two polaritons→XX→two outgoing polaritons'' is a coherent process. For relatively low optical intensities and within the first 10 to 20 ps after the sub-ps optical pump pulse, the resonantly coupled excitons, photons, and excitonic molecules form a conservative dynamical system in the optically active surface layer of high-quality bulk CdS (i.e., Hopfield's concept of a conservative exciton–photon system[1] is generalized in order to include excitonic molecules created by nonlinear two-photon absorption). As a result, the two basic processes, the coherent optical decay of excitonic molecules and propagation of the pump-/probe–pulse-induced polaritons in the optically active surface layer, determine the XX-mediated response, e.g., in a four-wave mixing (FWM) experiment.

In this work, we study the dynamics of an optically driven/decaying coherent ensemble of excitons, photons, and excitonic molecules in CdS and prove the validity of the bipolariton representation for a Wurtzite-type semiconductor at low bath temperatures. In Sec. II we outline the details of the experiment and discuss the relevant sample parameters. The concept of backward-scattering FWM is presented, and its sensitivity to different group velocities of lower and upper branch polaritons and excitonic molecules are illustrated. In Sec. III, by adapting an exactly solvable bipolariton model[17] to hexagonal CdS, we calculate the radiative decay rate $\Gamma_{\mathrm{rad}} = 1/\tau_{\mathrm{rad}}^{XX}$ of the molecule state. In Sec. IV the FWM signals observed at negative and positive delay times τ are analyzed separately. We show that the calculated radiative lifetime τ_{rad}^{XX} satisfies the condition $2\tau_{\mathrm{rad}}^{XX} \simeq T_2$, where T_2 is the dephasing time measured at $\tau < 0$, and, therefore, justify the bipolariton representation of excitonic molecules in CdS at low temperatures. We discuss the bipolariton distribution in

k space and show how it is mirrored in the spectral and temporal response of the FWM signal at positive delay times $\tau>0$. A short summary of the results is given in Sec. V.

II. EXPERIMENT

Four-wave mixing experiments in bulk semiconductors with strong exciton–photon interaction show signatures of both dephasing and propagation dynamics. When detecting the FWM signal in the backward-scattering geometry, the propagation and dephasing effects can be discriminated.[18] Here, we apply this geometry to exploit the strong differences in the group velocities of resonantly interacting upper branch polaritons, lower branch polaritons, and excitonic molecules in CdS.

A. Sample

CdS is a polar II–VI semiconductor of Wurtzite crystal lattice structure with a band gap energy of 2.582 eV at $T=4$ K. The transverse *A*-exciton energy at $\mathbf{k}=0$ is $E_T^A \simeq 2.5517$ eV and the longitudinal-transverse (LT) splitting amounts to $\hbar\omega_{\mathrm{LT}}\simeq 1.9$ meV. The reported values for the binding energy of the excitonic molecule ϵ^{XX} vary between 2.5 and 5.4 meV depending on the applied experimental techniques. Experiments based on two-photon processes yield values for ϵ^{XX} between 4.4 and 4.6 meV. $\epsilon^{XX}=2.5$ meV has been determined in magnetooptical experiments and $\epsilon^{XX}=5.4$ meV was obtained in photoluminescence measurements under high excitation by a pulsed N_2 laser.[19–24]

First studies of the coherent dynamics of polaritons in hexagonal CdS single crystals are presented in Ref. 25 using femtosecond transient and spectrally resolved four-wave mixing experiments. The observed similar size of linewidth and longitudinal-transverse splitting energy $\hbar\omega_{\mathrm{LT}}$ implies that only the polariton concept gives an adequate description of the coherent dynamics in CdS. Consequently, the coherent dynamics of excitonic molecules in CdS should also involve the resonant coupling of excitons and photons resulting in transverse and mixed polariton modes.[26–29]

The investigated high-quality CdS platelet with an in-plane crystal axis **c** and a thickness $d\simeq 2$ μm was mounted stress free in a helium cryostat. Reflections from the back surface were avoided by the wedge shape of the sample.

B. Four-wave mixing in backward-scattering geometry

In a FWM experiment with incoming pump and probe laser pulses of different delay times, the wave vectors $\mathbf{k}_1^{(0)}$ and $\mathbf{k}_2^{(0)}$ are not conserved at the crystal surface, i.e., the incoming photons induce a $\mathbf{k}_1$- ($\mathbf{k}_2$-) distribution of copropagating polaritons, which generally involves both branches of the polariton dispersion [i.e., the upper and lower polariton branches (UPB and LPB)], according to the pulse spectrum and energy position. For the delay time τ between the pump and probe pulse, two different regimes $\tau>0$ and $\tau<0$ have to be considered.

For negative delay times $\tau<0$ (i.e., the pump pulse arrives earlier than the probe pulse) the propagation dynamics does not influence the backward-scattered *XX*-mediated FWM signal because the group velocity of the optically generated molecules (bipolaritons) is small ($v_G^{XX}\leqslant 1.5\times 10^6$ cm/s), due to the absence of one-photon resonant coupling between excitonic molecules and the light field. This case allows us to examine the dephasing process of bipolaritons.

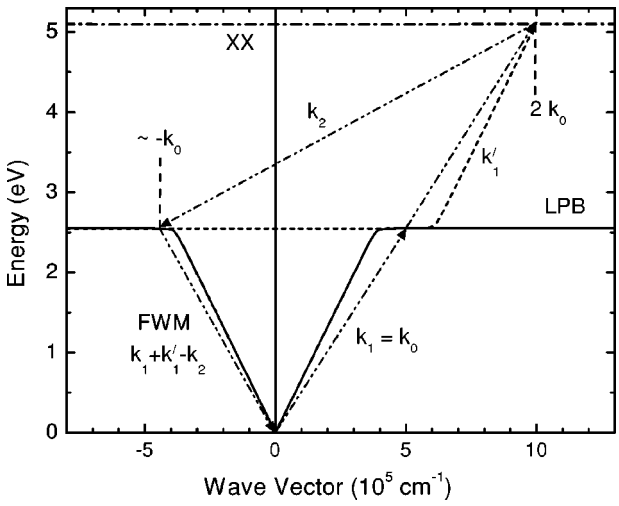

FIG. 1. Scheme of the optical transitions in **k** space generating the backward-scattered FWM signal at the energy of the bipolariton–polariton transition for the particular example of degenerate two-polariton excitation of excitonic molecules. Bipolaritons are excited by the LPB+LPB$\rightarrow XX$ process.

For positive delay times $\tau>0$, however, the propagation effects become important for the FWM dynamics, because the probe pulse excites polaritons with strongly frequency-varying group velocities. With increasing positive τ only the slowly propagating polaritons among those induced by the probe pulse are still staying in the surface layer at the time when the pump pulse arrives. In other words, the propagation dynamics segregates the polaritons: Upper branch polaritons with small $\mathbf{k}_2$ [$v_G^{\mathrm{POL}}(k_2=0)=0$] and lower branch polaritons with large wave vectors $\mathbf{k}_2$ [the smallest group velocity along the LPB is specified by $v_G^{\mathrm{POL}}(k_2=1.29\times 10^6\ \mathrm{cm}^{-1})=2.14\times 10^6$ cm/s] survive, while all other polaritons with high v_G^{POL} rapidly leave the optically active surface layer. The above scenario, which involves the coherent polaritons pinned in the surface layer, explains the molecule-mediated FWM signal at $\tau>0$ even by the lowest-order nonlinear susceptibility $\chi^{(3)}$.

In Fig. 1 we show the resonant polariton transitions involved in the *XX*-mediated FWM backward scattering for frequency-degenerate two-photon excitation of molecules. In this case an *XX* is created at $\mathbf{K}=2\mathbf{k}_0$ by resonant scattering of two lower-branch polaritons with $\mathbf{k}_1=\mathbf{k}_1'=\mathbf{k}_0$ (for CdS, $|\mathbf{k}_0|\simeq 5.1\times 10^5\ \mathrm{cm}^{-1}$). The FWM signal in the backward-scattering direction is induced by lower-branch polaritons with $\mathbf{k}_2\simeq 3\mathbf{k}_0$, according to the momentum-energy conservation law.

In our FWM setup the femtosecond pulses are generated by an optical parametric oscillator pumped by a Ti:Sa laser system. The Gaussian optical pulses of 18 meV spectral

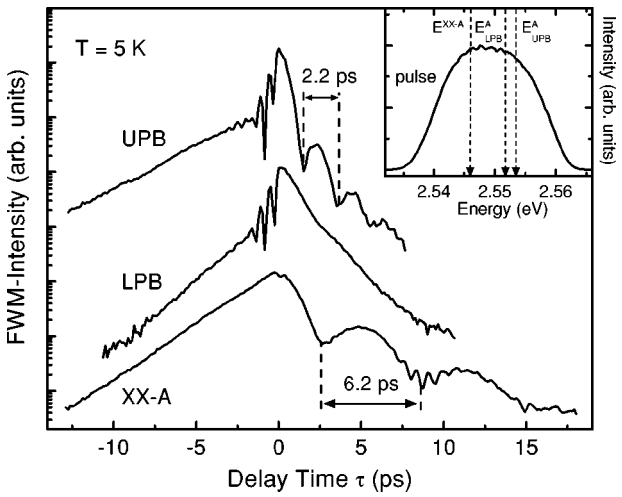

FIG. 2. The intensity of the TI backward-scattered FWM signal as a function of delay time τ. The FWM signal is measured at the energies of the UPB, LPB, and XX–A transition in bulk CdS at $T=5$ K. The curves are displaced for clarity. The inset shows the spectrum of the exciting laser pulses polarized $\mathbf{E}\perp\mathbf{c}$, centered at 2.549 eV with an intensity of $I_{\mathrm{pulse}}\simeq 64$ nJ/cm^2 and a bandwidth of 18 meV (FWHM).

width (FWHM) are centered at 2.549 eV and polarized $\mathbf{E}\perp\mathbf{c}$. Using a spectrometer and a CCD camera with 0.3 meV spectral resolution, we measure the time-integrated (TI) and spectrally resolved (SR) backscattered FWM signal as a function of delay time τ between the two pulses. Figure 2 shows the temporal FWM response measured in the backscattered direction at energy $E^{XX}-E_T^A$ (XX–A transition, where E^{XX} is the molecule energy) and at the energies E^A_{UPB} and E^A_{LPB} of the upper- and lower-branch polaritons. The large spectral width of the laser pulse (see the inset of Fig. 2) allows us to detect simultaneously the above-mentioned resonant transitions. For positive delay time $\tau>0$, the modulation of the UPB signal by a 2.2 ps-period stems from coherent polaritons sharply distributed at E_T^A and $E_T^A+\hbar\omega_{\mathrm{LT}}$. Thus the period of this oscillations is given by the LT-energy splitting of 1.9 meV. The fast oscillations at the UPB and LPB energies observed for -2 ps$<\tau<0$ are due to interference between the FWM signals associated with the XX and unbound two-polariton states, respectively.[2,30] The period of these oscillations yields the molecule binding energy $\epsilon^{XX}\simeq 5.1$ meV.

In the following analysis of the molecule-mediated FWM response, which proves the bipolariton picture for excitonic molecules in CdS, we focus on the FWM signals measured at the XX–A transition. Here the interesting signatures are (i) a slow exponential rise of the XX-mediated FWM signal at negative delay times, and (ii) a modulation of the XX–A signal with an oscillation period of 6.2 ps at positive delay times.

III. THE BIPOLARITON MODEL FOR EXCITONIC MOLECULES IN CADMIUM SULFIDE

The bipolariton model of excitonic molecules in Wurtzite-type semiconductors, such as CdS, deals with a quasibound state of two optically dressed excitons, which are interpreted in terms of both, transverse and mixed, polaritons. In this section we (i) characterize briefly transverse and mixed polariton modes and (ii) adapt the exactly solvable bipolariton model to molecules in CdS.

A. Transverse and mixed polaritons

The mixed and transverse polariton modes in low-temperature bulk CdS have been studied in experiments.[26–29] The optical transition to ground-state A excitons is forbidden in the $\mathbf{E}\|\mathbf{c}$ polarization and allowed for $\mathbf{E}\perp\mathbf{c}$, where $\mathbf{E}$ is the electric field vector. Thus in the spectral vicinity of the A-exciton line, the permittivity tensor $\varepsilon_{ij}(\omega,\mathbf{k})$ in the principal-axes coordinate system has only two independent components, $\varepsilon_{\|}(\omega,\mathbf{k})=\varepsilon_b$ and $\varepsilon_{\perp}(\omega,\mathbf{k})$, for $\mathbf{E}\|\mathbf{c}$ and $\mathbf{E}\perp\mathbf{c}$, respectively. Apart from the background dielectric constant ε_b, $\varepsilon_{\perp}(\omega,\mathbf{k})$ has also a resonant contribution from the A-exciton state. The tensor ε_{ij} gives rise to transverse and mixed polaritons with dispersions determined by

$$c^2k^2\equiv c^2(k_\perp^2+k_\|^2)=\omega^2[\varepsilon_b+4\pi\chi_\perp^A(k_\perp,k_\|,\omega)], \quad (1a)$$

$$c^2k_\|^2=[\omega^2-(c^2k_\perp^2)/\varepsilon_b][\varepsilon_b+4\pi\chi_\perp^A(k_\perp,k_\|,\omega)], \quad (1b)$$

respectively, where $k_\|$ ($k_\perp$) is the component of the polariton wave vector $\mathbf{k}$ along (perpendicular to) the main crystallographic axis $\mathbf{c}$. The exciton-mediated resonant susceptibility $\chi_\perp^A$ is given by $4\pi\chi_\perp^A=(\varepsilon_b\Omega_c^2)/[\omega_T^2+(\hbar\omega_T/M_\|)k_\|^2+(\hbar\omega_T/M_\perp)k_\perp^2-\omega^2]$, where $\hbar\omega_T=E_T^A(\mathbf{k}=0)$, $M_\|=2.85m_0$ and $M_\perp=0.9m_0$ are the longitudinal and transverse A-exciton masses, respectively, $\varepsilon_b=8.9$, and $\hbar\Omega_c=\hbar(2\omega_T\omega_{\mathrm{LT}})^{1/2}\simeq 98.5$ meV yields the polariton Rabi frequency for transverse modes.[31]

The dispersion Eqs. (1a)–(1b) yield the frequencies of transverse ($\omega^{\pm}_{\mathrm{trans}}$) and mixed ($\omega^{\pm}_{\mathrm{mix}}$) polaritons,

$$(\omega^{\pm}_{\mathrm{trans}})^2=[\omega^{\pm}_{\mathrm{trans}}(k_\perp,k_\|)]^2$$
$$=\tfrac{1}{2}[(\omega_x^2+\omega_\gamma^2+\Omega_c^2)$$
$$\pm[(\omega_x^2-\omega_\gamma^2+\Omega_c^2)^2+4\Omega_c^2\omega_\gamma^2]^{1/2}], \quad (2a)$$

$$(\omega^{\pm}_{\mathrm{mix}})^2=[\omega^{\pm}_{\mathrm{mix}}(k_\perp,k_\|)]^2$$
$$=\tfrac{1}{2}[(\omega_x^2+\omega_\gamma^2+\Omega_c^2)$$
$$\pm[(\omega_x^2-\omega_\gamma^2+\Omega_c^2)^2+4\Omega_c^2\omega_{\gamma\|}^2]^{1/2}], \quad (2b)$$

where $\omega^-(\omega^+)$ refers to the lower (upper) dispersion branch, $\omega_x^2=\omega_T^2+(\hbar\omega_T/M_\|)k_\|^2+(\hbar\omega_T/M_\perp)k_\perp^2$ and $\omega_\gamma^2=(c^2k^2)/\varepsilon_b$ are the A exciton and photon dispersions, respectively, and $\omega_{\gamma\|}^2=(c^2k_\|^2)/\varepsilon_b$. According to Eqs. (2a)–(2b), for $\mathbf{k}\|\mathbf{c}$ (i.e., $k_\perp=0$) the mixed polariton state is transverse ($\mathbf{E}\perp\mathbf{k}$) and $\omega^{\pm}_{\mathrm{mix}}=\omega^{\pm}_{\mathrm{trans}}$; for $\mathbf{k}\perp\mathbf{c}$ (i.e., $k_\|=0$) mixed polaritons decouple into transverse light and longitudinal excitons. The latter means that $\omega^{\pm}_{\mathrm{mix}}\to\omega_\gamma(k_\perp)$ and $\omega_x(k_\perp)+\omega_{\mathrm{LT}}$. In a general case, when the angle between the polariton wave vector $\mathbf{k}$ and the axis $\mathbf{c}$ is equal θ ($0<\theta<\pi/2$), the mixed polariton mode is neither purely transverse nor purely longitudinal, i.e., $0<\mathbf{k}\cdot\mathbf{E}<|\mathbf{k}||\mathbf{E}|$. Asymptotics of the polariton lower dispersion branches for $k\to\infty$ and fixed θ are given by $\omega^-_{\mathrm{trans}}(k\to\infty)\to\omega_T$ and $\omega^-_{\mathrm{mix}}(k\to\infty)\to\omega_T+\omega_{\mathrm{LT}}\sin^2\theta$. The asymptotics are important for the exactly

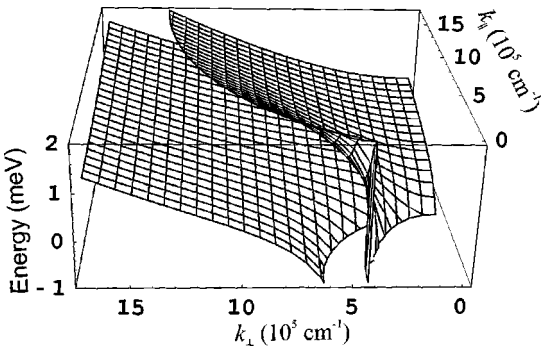

FIG. 3. The dispersion of lower-branch transverse polaritons, $E^{\mathrm{LPB}}_{\mathrm{trans}}(k_\perp,k_\parallel)-E^A_T(\mathbf{k}=0)$, and of lower-branch mixed polaritons, $E^{\mathrm{LPB}}_{\mathrm{mix}}(k_\perp,k_\parallel)-E^A_T(\mathbf{k}=0)$. The energies of transverse (the lower surface) and mixed (the upper surface) polaritons coincide at $\mathbf{k}=\{k_\parallel,k_\perp=0\}$.

solvable bipolariton model. The energies of lower-branch polaritons associated with the *A*-exciton resonance, $E^{\mathrm{LPB}}_{\mathrm{trans}}=\hbar\omega^{-}_{\mathrm{trans}}(k_\perp,k_\parallel)$ and $E^{\mathrm{LPB}}_{\mathrm{mix}}=\hbar\omega^{-}_{\mathrm{mix}}(k_\perp,k_\parallel)$, are plotted in Fig. 3.

B. Exactly solvable bipolariton model for excitonic molecules in CdS

The bipolariton model[2] interprets an excitonic molecule with the center-of-mass wave vector $\mathbf{K}$ as the bipolariton state which is characterized by the energy $\tilde{E}^{XX}(\mathbf{K})=E^{XX}(\mathbf{K})+\Delta_{\mathrm{rad}}(\mathbf{K})-(i/2)\Gamma_{\mathrm{rad}}(\mathbf{K})$. Here, $\Delta_{\mathrm{rad}}(\mathbf{K})$ and $\Gamma_{\mathrm{rad}}(\mathbf{K})$ are the radiative corrections, i.e., the Lamb shift and the radiative width of the *XX* state, respectively, and $E^{XX}(\mathbf{K})=2E^A_T(\mathbf{k}=0)-\epsilon^{XX}+\hbar^2K^2/2M_{XX}$ is the energy of the optically undressed molecule (M_{XX} is the molecule translational mass). Note that $\Delta_{\mathrm{rad}}(\mathbf{K})$ and $\Gamma_{\mathrm{rad}}(\mathbf{K})$ are the output parameters of the bipolariton model and should be found by solving the bipolariton wave equation. In order to adapt the exactly solvable bipolariton model[17] to excitonic molecules in optically highly anisotropic bulk CdS, we include equal contributions of transverse and mixed polariton modes to the total bipolariton wave function $\tilde{\Psi}$. Namely, according to the group theory study,[32] (i) the molecule wave function includes with equal probabilities the constituent excitons which give rise to transverse and mixed polaritons, and (ii) there is no quantum interference between the two decay pathes, i.e., the molecule decays either in two transverse or in two mixed outgoing polaritons. The latter means that $\Gamma_{\mathrm{rad}}=(1/2)\times[\Gamma^{\mathrm{trans}}_{\mathrm{rad}}(\mathbf{K})+\Gamma^{\mathrm{mix}}_{\mathrm{rad}}(\mathbf{K})]$, where $\Gamma^{\mathrm{trans}}_{\mathrm{rad}}/2$ and $\Gamma^{\mathrm{mix}}_{\mathrm{rad}}/2$ are the partial radiative rates of the photon-assisted resonant dissociation of the molecule into two transverse and two mixed polaritons, respectively.

The bipolariton wave equations for the molecule state constructed as a linear combination of two quasibound transverse polaritons ($i=$trans) and two quasibound mixed polaritons ($i=$mix), are given by

$$[E^{\mathrm{LPB}}_i(\mathbf{p}+\mathbf{K}/2)+E^{\mathrm{LPB}}_i(-\mathbf{p}+\mathbf{K}/2)]\tilde{\Psi}_i(\mathbf{p},\mathbf{K})+f_i(\mathbf{p},\mathbf{K})\sum_{\mathbf{p}'}W_{12}(\mathbf{p}-\mathbf{p}')\tilde{\Psi}_i(\mathbf{p}',\mathbf{K})=\tilde{E}^{XX}_i(\mathbf{K})\tilde{\Psi}_i(\mathbf{p},\mathbf{K}), \tag{3}$$

where $\mathbf{p}$ is the reduced relative momentum of two constituent polaritons, W_{12} is the Coulombic potential of exciton–exciton interaction,

$$f_i(\mathbf{p},\mathbf{K})=u^2_i(\mathbf{p}+\mathbf{K}/2)u^2_i(-\mathbf{p}+\mathbf{K}/2),$$

$$u^2_{\mathrm{trans}}(\mathbf{p})=[1+4\delta^2_{\mathrm{trans}}(\mathbf{p})/\Omega^2_c]^{-1},$$

$$u^2_{\mathrm{mix}}(\mathbf{p})=\{1+[1+\nu_{\mathrm{mix}}(\mathbf{p})][4\delta^2_{\mathrm{mix}}(\mathbf{p})/\Omega^2_c]\}^{-1},$$

$$\hbar\delta_i(\mathbf{p})=E^A_T(p_\perp,p_\parallel)-E^{\mathrm{LBP}}_i(p_\perp,p_\parallel),$$

and

$$\nu_{\mathrm{mix}}(\mathbf{p})=[(\hbar cp_\perp/\sqrt{\varepsilon_b})^2(\hbar cp_\parallel/\sqrt{\varepsilon_b})^2]/\{[E^{\mathrm{LPB}}_{\mathrm{mix}}(p_\perp,p_\parallel)]^2-(\hbar cp_\perp/\sqrt{\varepsilon_b})^2\}^2.$$

The bipolariton energy is given by

$$\tilde{E}^{XX}(\mathbf{K})=(1/2)(\tilde{E}^{XX}_{\mathrm{trans}}+\tilde{E}^{XX}_{\mathrm{mix}})=E_{XX}+(1/2)(\Delta^{\mathrm{trans}}_{\mathrm{rad}}+\Delta^{\mathrm{mix}}_{\mathrm{rad}})-(i/4)(\Gamma^{\mathrm{trans}}_{\mathrm{rad}}+\Gamma^{\mathrm{mix}}_{\mathrm{rad}}).$$

Equation (3) assumes (i) the excitonic representation of molecules and (ii) the leading contribution of lower-branch polaritons to the bipolariton wave function. The first assumption is valid if the ratio between the molecule and exciton binding energies is small, i.e., $\epsilon^{XX}/\epsilon^X\ll 1$ ($\epsilon^{XX}/\epsilon^X\simeq 0.18$ for CdS). While in our experiments the upper-branch polaritons do contribute to the stimulated *XX*-mediated scattering processes, their contribution to the spontaneous decay of molecules is of two to three orders of magnitude smaller than that due to lower-branch polaritons (see the detailed discussion of this question in Ref. 2). Thus the bipolariton wave Eq. (3) describes the Coulombically correlated relative motion of two polaritons (transverse and mixed) along the two energy sheets plotted in Fig. 3.

Being applied to hexagonal CdS, the exactly solvable bipolariton model (i) uses decoupling of the bipolariton wave functions into two parts, $\tilde{\Psi}_i=\Psi^{XX}_i+\delta\Psi_i$, where Ψ^{XX}_i is dominant at $|\mathbf{p}|\sim 1/a_{XX}\gg(\sqrt{\varepsilon_b}E^A_T)/(\hbar c)$ (a_{XX} is the molecule radius) and is determined by the Schrödinger equation for optically undressed excitons, and $\delta\Psi_i$ is dominant at the optical range $|\mathbf{p}|\leqslant(\sqrt{\varepsilon_b}E^A_T)/(\hbar c)$ and describes the outgoing (incoming) part of the wave function; (ii) needs a particular shape of the model potential of exciton–exciton interaction, $W_{12}(\mathbf{p})\propto\Psi^{XX}_i(\mathbf{p})$. The wave equations for Ψ^{XX}_i are given by

$$\left(\frac{\hbar^2p^2_\parallel}{M_\parallel}+\frac{\hbar^2p^2_\perp}{M_\perp}\right)\Psi^{XX}_{\mathrm{trans}}(\mathbf{p})+\sum_{\mathbf{p}'}W_{12}(\mathbf{p}-\mathbf{p}')\Psi^{XX}_{\mathrm{trans}}(\mathbf{p}')=-\epsilon^{XX}_{\mathrm{trans}}\Psi^{XX}_{\mathrm{trans}}(\mathbf{p}), \tag{4a}$$

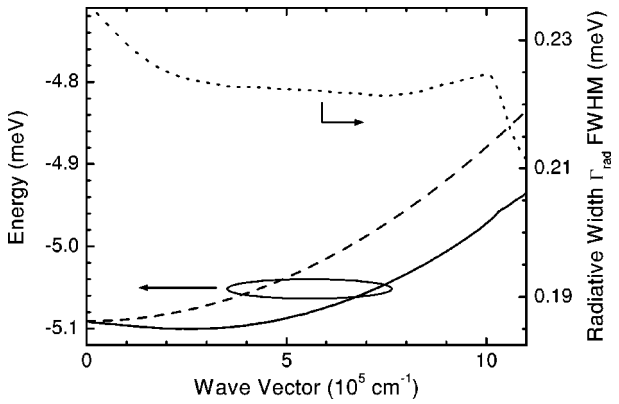

FIG. 4. Calculated radiative width and binding energies: bipolariton energy $-\epsilon^{XX}+\hbar^2K^2/2M_{XX}+\Delta_{\rm rad}(\mathbf{K})$ (solid line), shifted bare XX energy $-\epsilon^{XX}+\hbar^2K^2/2M_{XX}+\Delta_{\rm rad}(\mathbf{0})$ (dashed line), and $\Gamma_{\rm rad}(\mathbf{K})$ (dotted line).

$$\left(\frac{\hbar^2 p_\parallel^2}{M_\parallel}+\frac{\hbar^2 p_\perp^2}{M_\perp}\right)\Psi^{XX}_{\rm mix}(\mathbf{p})+\sum_{\mathbf{p}'} W_{12}(\mathbf{p}-\mathbf{p}')\Psi^{XX}_{\rm mix}(\mathbf{p}') + [\omega_{\rm LT}\sin^2\theta]\Psi^{XX}_{\rm mix}(\mathbf{p})=-\epsilon^{XX}_{\rm mix}\Psi^{XX}_{\rm mix}(\mathbf{p}), \tag{4b}$$

so that $\epsilon^{XX}=(1/2)(\epsilon^{XX}_{\rm trans}+\epsilon^{XX}_{\rm mix})$. While Eqs. (4a)–(4b) do not include the resonant polariton effects, the last term on the left-hand side of Eq. (4b) describes a ''staircase'' repulsive contact potential, which is due to the nonanalytic part of long-range electron-hole exchange interaction and can also be interpreted in terms of exciton–photon interaction. Equations (3) and (4a)–(4b) take into account the optical and electronic anisotropy effects in bulk CdS. By using a model deuteron potential of exciton–exciton interaction (attraction) and applying straightforwardly a method developed in Ref. 17, we calculate from Eqs. (3) and (4a)–(4b) the bipolariton radiative corrections, $\Delta_{\rm rad}(\mathbf{K})$ and $\Gamma_{\rm rad}(\mathbf{K})$. Thus the exactly solvable model simpifies the exciton–exciton interaction, but treats exactly, nonperturbatively the polariton effects. The control input parameter of the model is the binding energy ϵ^{XX} of a ''bare'' molecule.

In Fig. 4 we plot the energy $-\epsilon^{XX}+\hbar^2K^2/2M_{XX}+\Delta_{\rm rad}(\mathbf{K}=0)$ (dashed line) of optically undressed excitonic molecules, the bipolariton energy $-\epsilon^{XX}+\hbar^2K^2/2M_{XX}+\Delta_{\rm rad}(\mathbf{K})$ (solid line), and the bipolariton radiative width $\Gamma_{\rm rad}(\mathbf{K})$ (dotted line) calculated for $\mathbf{K}\perp\mathbf{c}$. The strength of exciton–exciton Coulombic interaction is adjusted to give the input XX binding energy $\epsilon^{XX}=4.87$ meV so that the optically renormalized binding energy $\epsilon^{XX}-\Delta_{\rm rad}(\mathbf{K}=0)=5.08$ meV, i.e., reproduces the value of about 5.1 meV found in our experiments. The curve $\Gamma_{\rm rad}=\Gamma_{\rm rad}(|\mathbf{K}|)$ has a spike at $|\mathbf{K}|\simeq 10.2\times10^5$ cm^{-1} (see the dotted line in Fig. 4), which is due to a van Hove singularity in the energy-momentum conservation law for the frequency- and wave-vector-degenerate two-polariton generation/decay of excitonic molecules ($\hbar\omega_1=\hbar\omega_2=E^{XX}/2$ and $\mathbf{k}_1=\mathbf{k}_2=\mathbf{K}/2$)[2]. The van Hove singularity refers to the path ''$XX\leftrightarrow$two transverse polaritons''; the path ''$XX\leftrightarrow$two mixed polaritons'' has no van Hove singularity for $\mathbf{K}\perp\mathbf{c}$. The singularity gives rise to the so-called ''Mexican hat structure'' in the bipolariton energy (see the solid line in Fig. 4). The latter structure caused by the radiative renormalizations is, however, beyond the resolution of our experiment.

For $|\mathbf{K}|\leqslant 10^6$ cm^{-1} the radiative width $\Gamma_{\rm rad}\simeq 0.23$ meV, which is only weakly dependent on the wave vector $\mathbf{K}$, yields the XX radiative lifetime $\tau^{XX}_{\rm rad}=\hbar/\Gamma_{\rm rad}\simeq 2.8$ ps. In our experiments the signal optical pulses are induced by transverse polaritons with $\mathbf{k}\perp\mathbf{c}$ and propagating in the backward-scattering direction. However, the XX radiative corrections, $\Delta_{\rm rad}(\mathbf{K})$ and $\Gamma_{\rm rad}(\mathbf{K})$, include all possible polarizations and propagation directions of outgoing polaritons in the decay paths ''$XX\rightarrow$two transverse or two mixed polaritons.''

The large difference of the XX radiative lifetimes in CdS and CuCl ($\tau^{XX}_{\rm rad}\simeq 3$ ps in CdS versus $\tau^{XX}_{\rm rad}\simeq 20$ ps in CuCl) correlates with the considerable difference of the molecule binding energies in these materials ($\epsilon^{XX}\simeq 5$ meV in CdS versus $\epsilon^{XX}\simeq 32$ meV in CuCl): With decreasing ϵ^{XX} the bipolariton wave function $\tilde{\Psi}$ becomes more concentrated in the optical range resulting in the increase of $\Gamma_{\rm rad}$.

IV. EXPERIMENTAL RESULTS AND DISCUSSION

In this section the coherent dynamics in an optically driven ensemble of excitons, photons, and excitonic molecules is studied by analyzing the rise/decay times and period of oscillations of the FWM signal at the XX–A, UPB, and LPB transitions (see Fig. 2). From the measured rise time of the FWM signal at $\tau\leqslant 0$ we estimate the bipolariton dephasing time T_2 for the temperature $T\rightarrow 0$. The complicated line shape of the time-integrated (TI) signal at $\tau\geqslant 0$ is attributed to the transient coherent dynamics of optically induced polaritons and bipolaritons.

A. FWM signal at $\tau<0$

At negative delay time τ, bipolaritons are excited by two photons $\mathbf{k}_1$ of the pump pulse, and the FWM signal is caused by pump-induced two-photon coherence. According to Fig. 2, the fast oscillations at the UPB and LPB energies disappear rapidly with increasing $|\tau|$, due to fast dephasing caused by destructive interference between the XX state and the two-polariton continuum. The FWM signal itself, however, persists and shows an exponential decrease with increasing $|\tau|$. As explained in Sec. II B, the observed dynamics in this delay-time regime is determined only by dephasing of the XX states. Thus the temperature-dependent bipolariton dephasing time T_2 can directly be obtained from the measured rise time $\tau^{\rm FWM}_{\rm rise}$ at the XX–A transition. The dephasing spectral width is given by $\Gamma_{\rm dec}(T)=\hbar/\tau^{\rm FWM}_{\rm rise}(T)=2\hbar/T_2(T)$.

In Fig. 5 we plot the TI backward-scattered FWM signal detected at the energy of the XX–A transition for three different temperatures. It clearly shows an increase of the dephasing (decay) width, i.e., decrease of $\tau^{\rm FWM}_{\rm rise}$, with increasing temperature. Our measurements yield $T_2(T=5\ {\rm K})\simeq 4.0$ ps and $\Gamma_{\rm dec}(T=5\ {\rm K})\simeq 0.33$ meV. In order to estimate the zero-temperature limit $\Gamma_{\rm dec}(T=0\ {\rm K})$ we measure the decay width in the temperature range between 5 K and 20 K (see Fig. 5). In order to estimate the zero-temperature limit

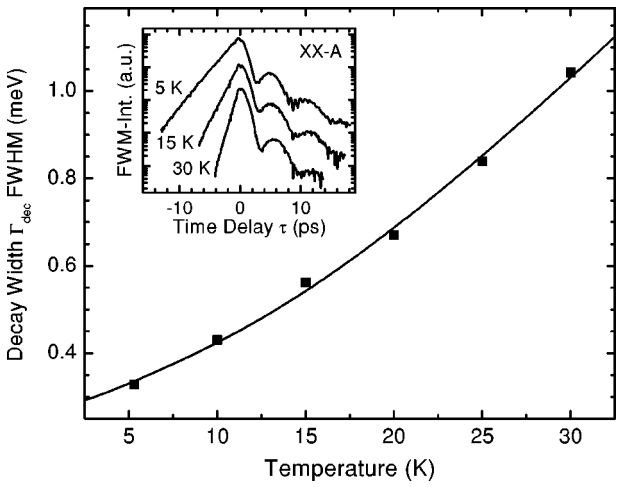

FIG. 5. Experimental determination of the radiative decay width $\Gamma_{\mathrm{dec}}(T)$ of the molecule-mediated FWM signal at the energy of the XX–A transition from the exponential rise time at negative delay times. We find $\Gamma_{\mathrm{dec}}(0\ \mathrm{K})=0.28$ meV by fitting the experimental data as explained in the text (solid line). The inset shows the TI backward-scattered FWM signal detected at the energy of the XX–A transition for three different temperatures.

of Γ_{dec} we fit the experimental data by $\Gamma_{\mathrm{dec}}(T)=\Gamma_{\mathrm{dec}}(T=0\ \mathrm{K})+C/[\exp(\Delta E/k_BT)-1]$, according to the procedure developed in Ref. 11. The relevant temperature-dependent scattering process is the absorption of LA phonons by molecules. The interaction strength C and zero-temperature dephasing width $\Gamma_{\mathrm{dec}}(T=0\ \mathrm{K})$ are the fitting parameters, and the phonon energy $\Delta E=2M_{XX}v_{LA}^2\simeq 0.5$ meV (v_{LA} is the longitudinal sound velocity). Finally, we find $C\simeq 0.11$ meV, $\Gamma_{\mathrm{dec}}(T=0\ \mathrm{K})\simeq 0.28$ meV, and $T_2(T=0\ \mathrm{K})\simeq 4.8$ ps.

The comparison with the theoretically predicted XX radiative lifetime of 2.8 ps, which yields $T_2\simeq 5.6$ ps in the $T_2=2T_1=2\tau_{\mathrm{rad}}^{XX}$ limit, clearly demonstrates that the radiative decay of molecules gives the absolutely dominant contribution to $\Gamma_{\mathrm{dec}}(T=0\ \mathrm{K})$. No significant changes of the decay time with increasing exciton density in the range between 5×10^{14} and 10^{16} cm^{-3} are found. Thus for the used low-intensity optical excitations the exciton–exciton scattering process is weak and practically does not contribute to Γ_{dec}. We attribute the small difference between Γ_{rad} and $\Gamma_{\mathrm{dec}}(T=0\ \mathrm{K})$ to spontaneous emission of LA phonons from the optically populated XX states $|\mathbf{K}|\geqslant(M_{XX}v_{LA})/\hbar\simeq 6.6\times 10^5$ cm^{-1} (in our case the optically generated molecules are widely distributed in the band 10^6 $\mathrm{cm}^{-1}\leqslant|\mathbf{K}|\leqslant 3\times 10^6$ cm^{-1}, see below Fig. 8). Therefore $\Gamma_{\mathrm{dec}}(T=0\ \mathrm{K})$ is given by $\Gamma_{\mathrm{dec}}(T=0\ \mathrm{K})=\Gamma_{\mathrm{rad}}+\Gamma_{\mathrm{LA}}^{XX}(T=0\ \mathrm{K})$, i.e., $2/T_2=1/\tau_{\mathrm{rad}}^{XX}+1/\tau_{LA}^{XX}$, where τ_{LA}^{XX} is a characteristic time for spontaneous emission of LA-phonons. The estimated value $\tau_{LA}^{XX}\simeq 12.5$ ps is in a good agreement with a time-scale relevant to exciton- (biexciton-) LA-phonon scattering at low temperatures.[15,16]

B. FWM signal at $\tau>0$

In order to explain the observed oscillations with 6.2 ps period in the TI backward-scattered FWM signal detected at the XX–A transition for positive delay times (see Fig. 2), we analyze experimentally and theoretically the temporal behavior of the bipolariton distribution in $\mathbf{k}$ space (Figs. 6–8). The spectrally resolved FWM response is plotted in Fig. 6 for various delay times τ between 0 ps and +10 ps. At very early delay times the signal arises from the interaction of all polaritons induced by the laser pulses. For $\tau>1$ ps two spectral peak develop at the E_{LPB}^{A} and E_{UPB}^{A} polariton transitions. In this case the FWM signal is due to the interference grating induced by the first and second laser pulses and can be described as a $+\mathbf{k}_1-\mathbf{k}_2+\mathbf{k}_1'$ third-order scattering process. For delay times $\tau>3$ ps the FWM signal at the XX–A transition, which can be specified as $+\mathbf{k}_1+\mathbf{k}_1'-\mathbf{k}_2$ XX-mediated scattering, dominates over that at E_{LPB}^{A} and E_{UPB}^{A} energies. A double-peak structure (energies E_1^{XX-A} and E_2^{XX-A}) with the energy splitting of 0.7 meV is observed.

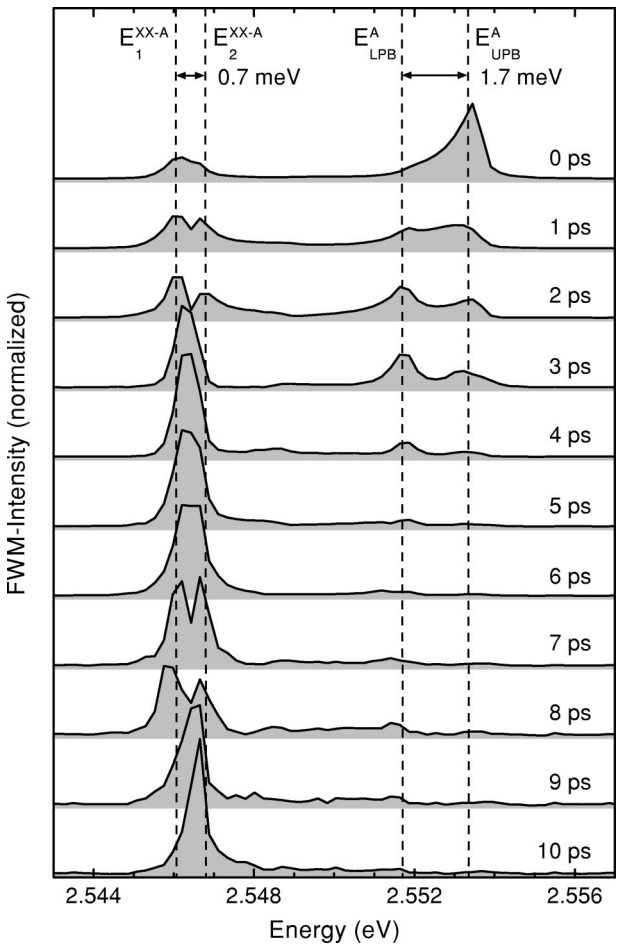

FIG. 6. The intensity of the SR backward-scattered FWM signal at various positive delay times τ between 0 ps and 10 ps. The curves are displaced for clarity. Each spectrum is normalized to the spectrally integrated FWM intensity.

As already explained in Sec. II B, for $\tau>0$ only polaritons with a small group velocity v_G^{POL} contribute to the backward-scattered FWM signal from the thin optically active layer and give rise to the observed peaks at $E_{\mathrm{LPB}}^{A}\simeq E_T^A$ and $E_{\mathrm{UPB}}^{A}\simeq E_T^A+\hbar\omega_{\mathrm{LT}}$. This behavior can be visualized with the help of Fig. 7 where the calculated energy distribution of upper-

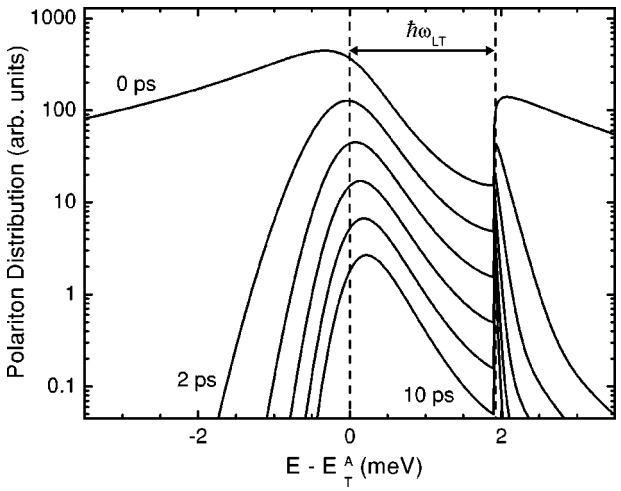

FIG. 7. The calculated energy distribution of upper- and lower-branch polaritons contributing to the backward-scattered FWM signal calculated for different positive delay times between $\tau=0$ ps and 10 ps in steps of 2 ps. The thickness of the surface layer, optically active in backward-scattering FWM, is about $1/K_X^{\max}$, where the resonant absorption coefficient associated with *A* excitons in CdS is given by $K_X^{\max}\simeq 2\times 10^5$ cm^{-1}. In the calculations the Pekar additional boundary condition is used.

and lower-branch polaritons in the optically active surface layer is plotted for various delay times between 0 ps and 10 ps after the first laser pulse. The above calculations of the energy distribution refer to Pekar's additional boundary condition (ABC).[31] The distribution shows two distinct peaks at the energies $\simeq E_T^A$ (caused by lower-branch polaritons with small $v_G^{\rm POL}$, i.e., $|\mathbf{k}|>\mathbf{k}_0$) and $\simeq E_T^A+\hbar\omega_{\rm LT}$ (caused by upper-branch polaritons with small $v_G^{\rm POL}$, i.e., $|\mathbf{k}|\simeq 0$). Note that the peak at $\simeq E_T^A$ shifts to slightly larger energies with increasing delay time, whereas the peak at $E_T^A+\hbar\omega_{\rm LT}$ does not change its position. As a result, the energy difference

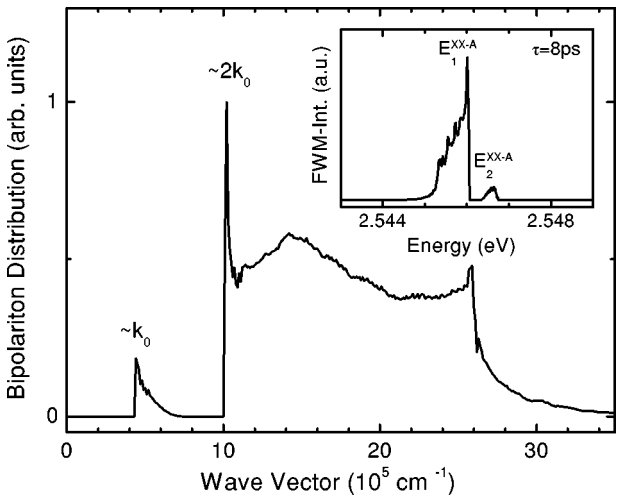

FIG. 8. The calculated distribution function $N_{XX}(\mathbf{K}=\mathbf{k}_1+\mathbf{k}_1')$ of hot *XX*s (bipolaritons) generated by the first laser pulse $\mathbf{k}_1^{(0)}$. The inset shows the calculated spectral response of the FWM signal at the *XX*–*A* transition in backward-scattered direction derived from $N_{XX}(\mathbf{K})$ for a delay time of 8 ps.

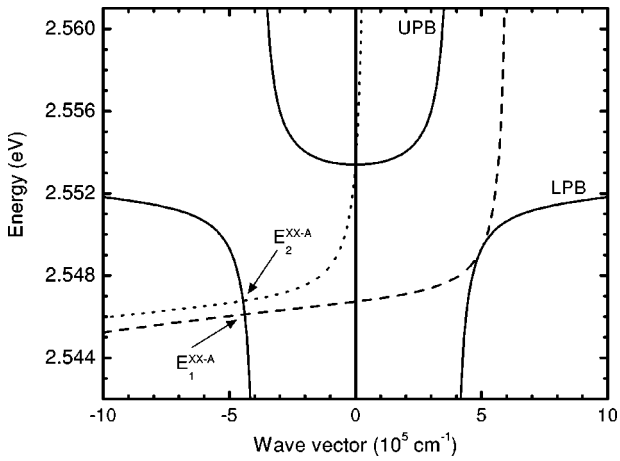

FIG. 9. Graphic solution of the energy-momentum conservation law to determine the energy of the backscattered FWM response at the *XX*–*A* transition. The spectral point marked by $E_1^{XX-A}(E_2^{XX-A})$ originates from the induced transition from *XX*s with wave vector $\simeq 2\mathbf{k}_0(\simeq\mathbf{k}_0)$ by LPBs.

between the two peaks decreases from $\hbar\omega_{\rm LT}=1.9$ meV to approximately 1.7 meV for 10 ps delay time. This explains the energy difference $E_{\rm UPB}^A-E_{\rm LPB}^A\simeq 1.7$ meV observed for SR FWM signal at $\tau>0$ (see Fig. 6).

We attribute the double-peaked structure at the *XX*–*A* transition in Fig. 6 to a hot, unrelaxed distribution of excitonic molecules optically generated by the pump pulse. In order to prove this interpretation we calculate the *XX* distribution function $N_{XX}(\mathbf{K})$ for molecules resonantly created in the optically active surface layer by the first laser pulse with the bipolariton model (see Fig. 8). The numerical evaluations deal with the basic process "polariton $\mathbf{k}_1$+polariton $\mathbf{k}_1'$ $\rightarrow XX$ $(\mathbf{K}=\mathbf{k}_1+\mathbf{k}_1')$" and Pekar's ABC for optically induced incoming polaritons. The sharp spike in the distribution function $N_{XX}(\mathbf{K})$ at $\mathbf{K}=2\mathbf{k}_0$ is due to the frequency-degenerate two-polariton generation of molecules, as illustrated in Fig. 1. The broad distribution of *XX*s at $|\mathbf{K}|\geqslant 2|\mathbf{k}_0|$ originates from the excitation path "LBP+LBP$\rightarrow XX$," and the narrow distribution at $|\mathbf{K}|\simeq|\mathbf{k}_0|$ is due to the excitation path "UBP+LBP$\rightarrow XX$," respectively. In the inset of Fig. 8 we show the calculated backward-scattered SR FWM signal at $\tau=+8$ ps from the optically induced distribution $N_{XX}(\mathbf{K})$. The hot molecules, distributed in the two separate bands at $\mathbf{K}\simeq\mathbf{k}_0$ and $\mathbf{K}\geqslant 2\mathbf{k}_0$, give rise to the FWM signal at the energies E_2^{XX-A} and E_1^{XX-A} in agreement with the observation of the double-peaked spectrum (see Fig. 6, the curve which refers to 8 ps time delay).

The formation of the resonant FWM signals in the backward-scattering direction at E_1^{XX-A} and E_2^{XX-A} is illustrated in Fig. 9 by the graphic solution of the energy-momentum conservation law in two-polariton generation/decay of the molecules. The observed energy of the FWM signal is given by $E_i^{XX-A}=E_{\rm LPB}^A(\mathbf{k}_1+\mathbf{k}_1'-\mathbf{k}_2)=\tilde{E}^{XX}(\mathbf{k}_1+\mathbf{k}_1')-E_{\rm LPB}^A(\mathbf{k}_2)$, where $E_{\rm LPB}^A(\mathbf{k})$ is the dispersion of the lower polariton branch and $i=1,2$ (see also Fig. 1). For $i=1$ one has $|\mathbf{k}_1+\mathbf{k}_1'|\simeq 2|\mathbf{k}_0|$ and $|\mathbf{k}_2|\simeq 3|\mathbf{k}_0|$, for $i=2$ we approximate $|\mathbf{k}_1+\mathbf{k}_1'|\simeq|\mathbf{k}_0|$ and $|\mathbf{k}_2|\simeq 2|\mathbf{k}_0|$. In the both

cases the FWM signal is generated at $\mathbf{k} \simeq -\mathbf{k}_0$. In order to determine E_i^{XX-A} and the energy of low-branch polaritons which induce the $XX-A$ transition at $E^A_{\mathrm{LPB}}(\mathbf{k}_2)$, we plot the inverted dispersion of the lower polariton branch with the origin point placed at the bipolariton energy $\tilde{E}^{XX}(\mathbf{k}_1+\mathbf{k}_1' \simeq 2\mathbf{k}_0)$ and $\tilde{E}^{XX}(\mathbf{k}_1+\mathbf{k}_1' \simeq \mathbf{k}_0)$ by the dotted and dashed curves, respectively. The resonant energies are given by the intersection of these curves with the lower polariton branch and marked by the arrows. The values of E_1^{XX-A} and E_2^{XX-A} are in a good agreement with the peak energies of the experimentally found and theoretically calculated FWM spectrum (see Fig. 6 and the inset of Fig. 8). With the help of this analysis the oscillation at $\tau > 0$ for the $XX-A$ transition observed in the TI backscattered FWM signal (Fig. 2) can be explained by the interference of the two polaritons which induce the FWM signal. Their energy difference $E^A_{\mathrm{LPB}}(\mathbf{k}_2 \simeq 3\mathbf{k}_0) - E^A_{\mathrm{LPB}}(\mathbf{k}_2 \simeq 2\mathbf{k}_0) \simeq 0.6$ meV nicely agrees with the measured oscillation period of 6.2 ps.

C. Bipolariton *k*-space dispersion and *k*-dependent dephasing times

In this subsection we will finally shortly comment on the influence of the bipolariton $\mathbf{k}$ vector on the observed risetimes in TI backscattered FWM signals detected at different energies. The preceding discussion in this section showed, that the dephasing time T_2 of bipolaritons with wave vector $\simeq \mathbf{k}_0$ ($\simeq 2\mathbf{k}_0$) can be determined when the TI backscattered FWM signal at negative delay times $\tau < 0$ is directly detected at the energy E_2^{XX-A} (E_1^{XX-A}) of the $XX-A$ transition. As the FWM signal at the $XX-A$ transition in Fig. 2 is averaged over both of the two resonances, we determined an averaged dephasing time T_2 (respectively, decay width Γ_{dec}) in Fig. 5. In Fig. 10 we show the TI backscattered FWM response measured separately at the energies E_1^{XX-A} and E_2^{XX-A} for $\tau < 0$ at a temperature of $T = 5$ K yielding two different dephasing times $T_2(\mathbf{K} \simeq \mathbf{k}_0) = 5.4$ ps and $T_2(\mathbf{K} \simeq 2\mathbf{k}_0) = 3.5$ ps. The radiative lifetime of bipolaritons at $\simeq 2\mathbf{k}_0$ is smaller than that for bipolaritons at $\simeq \mathbf{k}_0$.

The observed difference in these two dephasing times can be explained as followed. First of all, the calculated radiative width $\Gamma_{\mathrm{rad}}(\mathbf{K} \simeq 2\mathbf{k}_0)$ is slightly larger than $\Gamma_{\mathrm{rad}}(\mathbf{K} \simeq \mathbf{k}_0)$ (see Fig. 4), and thus T_2 is slightly smaller for bipolaritons with wave vector $\mathbf{K} \simeq 2\mathbf{k}_0$ than for bipolaritons with $\mathbf{K} \simeq \mathbf{k}_0$. Second, bipolaritons at $\mathbf{K} \simeq 2\mathbf{k}_0$ can be scattered on the bipolariton dispersion relation by LA phonons whereas this is not possible for bipolaritons at $\mathbf{K} \simeq \mathbf{k}_0$. Considering only the E_1^{XX-A} transition, the agreement with the theory is even better than for the averaged dephasing time.

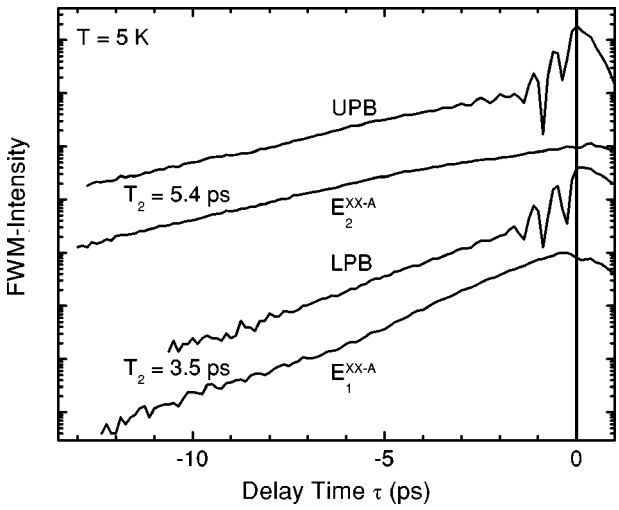

FIG. 10. The intensity of the TI backward-scattered FWM signal for negative delay times $\tau < 0$. The FWM signal is measured at the energies of the UPB, LPB, and at the two resonances E_1^{XX-A} and E_2^{XX-A} of the $XX-A$ transition at $T = 5$ K. The curves are displaced for clarity.

We plot in Fig. 10 the FWM signal at $\tau < 0$ detected at the energies of the LPB and the UPB for comparison. After the fast oscillations disappeared due to the dephasing of the excited unbound two-polariton states, a slowly exponentially rising signal generated by bipolaritons remains. At the energy of the LPB (UPB) we estimate approximately the same dephasing time T_2 than at the energy $E_1^{XX-A}(E_2^{XX-A})$ of the $XX-A$ transition thus confirming that bipolaritons with wave vector $\mathbf{K} \simeq 2\mathbf{k}_0(\mathbf{K} \simeq \mathbf{k}_0)$ contribute to the corresponding FWM signal.

V. SUMMARY

In conclusion, by FWM experiments in the backward-scattering geometry, we have proved the validity of the bipolariton picture for excitonic molecules in high-quality bulk CdS at low bath temperatures. The exactly solvable bipolariton model, adapted to this optically anisotropic semiconductor, clearly shows that the risetime of the XX-mediated FWM signal is mainly determined by the radiative decay of excitonic molecules with $\tau_{\mathrm{rad}}^{XX} \simeq 2.8$ ps.

ACKNOWLEDGMENTS

Support of this work by the DFG and EPSRC is gratefully acknowledged.

[1] J. J. Hopfield, Phys. Rev. **112**, 1555 (1958).
[2] A. L. Ivanov, H. Haug, and L. V. Keldysh, Phys. Rep. **296**, 237 (1998).
[3] A. Mysyrowicz, J. B. Grun, R. Levy, A. Bivas, and S. Nikitine, Phys. Lett. **26A**, 615 (1968).
[4] B. Hönerlage, R. Lévy, J. B. Grun, C. Klingshirn, and K. Bohnert, Phys. Rep. **124**, 161 (1985).
[5] U. Neukirch, S. R. Bolton, N. A. Fromer, L. J. Sham, and D. S. Chemla, Phys. Rev. Lett. **84**, 2215 (2000).
[6] P. Borri, W. Langbein, U. Woggon, J. R. Jensen, and J. M. Hvam,

Phys. Rev. B **62**, R7763 (2000).
[7] E. M. Goldys, G. C. La Rocca, and F. Bassani, Phys. Rev. B **61**, 10 346 (2000).
[8] T. Baars, G. Dasbach, M. Bayer, and A. Forchel, Phys. Rev. B **63**, 165311 (2001).
[9] D. S. Chemla, A. Maruani, and E. Batifol, Phys. Rev. Lett. **42**, 1075 (1979).
[10] N. Nagasawa, M. Kuwata, E. Hanamura, T. Itoh, and A. Mysyrowicz, Appl. Phys. Lett. **55**, 1999 (1989).
[11] H. Akiyama, T. Kuga, M. Matsuoka, and M. Kuwata-Gonokami, Phys. Rev. B **42**, 5621 (1990).
[12] E. Tokunaga, A. L. Ivanov, S. V. Nair, and Y. Masumoto, Phys. Rev. B **63**, 233203 (2001); E. Tokunaga, K. Kurihara, M. Baba, Y. Masumoto, and M. Matsuoka, Phys. Rev. B **64**, 045209 (2001).
[13] M. Ueta, H. Kanzaki, K. Kobayashi, Y. Toyozawa, and E. Hanamura, *Excitonic Processes in Solids*, Springer Series in Solid-State Sciences, Vol. 60 (Springer, Berlin, 1986), Chaps. 2 and 3.
[14] J. Wicksted, M. Matsushita, H. Z. Cummins, T. Shigenari, and X. Z. Lu, Phys. Rev. B **29**, 3350 (1984).
[15] J. Shah, *Ultrafast Spectroscopy of Semiconductors and Semiconductor Nano-structures*, Springer Series in Solid-State Sciences, Vol. 115 (Springer, Berlin, 1996).
[16] C. F. Klingshirn, *Semiconductor Optics* (Springer, Berlin, 1997), Chap. 22.
[17] A. L. Ivanov and H. Haug, Phys. Rev. Lett. **74**, 438 (1995).
[18] U. Woggon, W. Langbein, Ch. Mann, F. Gindele, and A. L. Ivanov, Phys. Status Solidi B **221**, 467 (2000).
[19] S. Shionoya H. Saito, E. Hanamura, and O. Akimoto, Solid State Commun. **12**, 223 (1973).
[20] J. Voigt and I. Rückmann, Phys. Status Solidi B **61**, K85 (1974).
[21] J. M. Hvam, Solid State Commun. **26**, 373 (1978).
[22] Y. Nozue, T. Itoh, and M. Ueta, J. Phys. Soc. Jpn. **44**, 1305 (1978).
[23] B. S. Rasbirin, I. N. Uraltsev, and G. V. Mikhailov, Solid State Commun. **25**, 799 (1978).
[24] J. Puls, I. Rückmann, and J. Voigt, Phys. Status Solidi B **96**, 641 (1979).
[25] D. Weber, W. Petri, U. Woggon, C. Klingshirn, S. Shevel, and E. O. Göbel, Phys. Rev. B **55**, 12 848 (1997).
[26] J. J. Hopfield and D. G. Thomas, Phys. Rev. **122**, 35 (1961).
[27] S. A. Permogorov, A. V. Sel'kin, and V. V. Travnikov, Fiz. Tverd. Tela **15**, 1822 (1973) [Sov. Phys. Solid State **15**, 1215 (1973)].
[28] I. Broser, M. Rosenzweig, R. Broser, M. Richard, and E. Birkicht, Phys. Status Solidi B **90**, 77 (1978).
[29] I. Broser, R. Broser, E. Beckmann, and E. Birkicht, Solid State Commun. **39**, 1209 (1981).
[30] Th. Östreich, K. Schönhammer, and L. J. Sham, Phys. Rev. Lett. **74**, 4698 (1995).
[31] C. Weisbuch and R.G. Ulbrich, in *Light Scattering in Solids III*, Vol. 51 of Topics in Applied Physics, edited by M. Cardona and G. Güntherodt (Springer, Berlin, 1982), p. 207.
[32] F. Bassani, J. J. Forney, and A. Quattropani, Phys. Status Solidi B **65**, 591 (1974).